Tectonophysics 728–729 (2018) 119–129

Contents lists available at ScienceDirect

Tectonophysics

journal homepage: www.elsevier.com/locate/tecto

Role of erosion and isostasy in the Cordillera Blanca uplift: Insights from landscape evolution modeling (northern Peru, Andes)

Audrey Margirier[a,b,*], Jean Braun[a], Xavier Robert[b], Laurence Audin[b]

[a] Helmholtz-Zentrum Potsdam, GeoForschungsZentrum (GFZ) Potsdam, Potsdam, Germany
[b] Université Grenoble, Alpes, CNRS, IRD, ISTerre, 38000 Grenoble, France

ARTICLE INFO

Keywords:
Rock uplift
Isostatic effect of eroding a denser rock mass
Normal fault
Low-temperature thermochronology
Numerical modeling of the landscape evolution
Cordillera Blanca
Peruvian Andes

ABSTRACT

The processes driving uplift and exhumation of the highest Peruvian peaks (the Cordillera Blanca) are not well understood. Uplift and exhumation seem closely linked to the formation and movement on the Cordillera Blanca normal fault (CBNF) that delimits and shapes the western flank of the Cordillera Blanca. Several models have been proposed to explain the presence of this major normal fault in a compressional setting, but the CBNF and the Cordillera Blanca recent rapid uplift remain enigmatic. Whereas the Cordillera Blanca morphology demonstrates important erosion and thus a significant mass of rocks removal, the impact of erosion and isostasy on the evolution of the Cordillera Blanca uplift rates has never been explored. We address the role of erosion and associated flexural rebound in the uplift and exhumation of the Cordillera Blanca with numerical modeling of landscape evolution. We perform inversions of the broad features of the present-day topography, total exhumation and thermochronological data using a landscape evolution model (FastScape) to provide constraints on the erosion efficiency factor, the uplift rate and the temperature gradient. Our results evidence the not negligible contribution of erosion and associated flexural rebound to the uplift of the Cordillera Blanca and allow us to question the models previously proposed for the formation of the CBNF.

1. Introduction

In mountain ranges, surface uplift is usually assumed to be the result of shortening and crustal thickening. Surprisingly, in northern Peru, uplift of the footwall of an active normal fault is responsible for the formation of the highest Peruvian summits in the Cordillera Blanca (Fig. 1). Several models have been proposed (Dalmayrac and Molnar, 1981; McNulty and Farber, 2002) to explain this unusual situation, but the processes driving both the Cordillera Blanca uplift and extensional deformation along the Cordillera Blanca normal fault (CBNF) remain poorly constrained. The CBNF trends parallel to the Andean range and is the most spectacular normal fault in the Andes (Fig. 1; Margirier et al., 2017): the CBNF is ~200 km long and shows ~7 km of vertical offset in total (Margirier et al., 2016), it has been active since ~5.4 Ma (Bonnot, 1984; Giovanni, 2007). The CBNF is located above the Peruvian flat-slab (Barazangi and Isacks, 1976), a section of the convergent plate boundary between the Nazca Plate and the South American Plate characterized today by near-horizontal subduction geometry. The Cordillera Blanca and the Cordillera Negra form, respectively, the hanging wall and the footwall of the CBNF (Fig. 1).

The Cordillera Blanca fast exhumation rate (~1 mm/yr) has been previously linked to motion on the CBNF (e.g., Bonnot, 1984; McNulty and Farber, 2002; Giovanni, 2007; Margirier et al., 2015). New thermobarometry data and erosion rates reconstruction based on thermochronological data indicate a recent, i.e. Early Pleistocene, increase in erosion rate in the Cordillera Blanca (~2–0 Ma; Margirier et al., 2016). Margirier et al. (2016) suggested that an important isostatic contribution from glacial erosion may explain the recent exhumation of the Cordillera Blanca batholith. Indeed, the removal of such a mass of material represents a significant upward unloading on the lithosphere, which should drive substantial flexural uplift. This unloading and flexural uplift would have also generated large differential stresses in the lithosphere, which could have caused the reactivation of pre-existing structures such as the CBNF. Previous studies demonstrated that the flexural uplift driven by alpine-type valley incision could reach rates similar to those caused by tectonic processes (Montgomery, 1994; Small and Anderson, 1995; Cederbom et al., 2004; Stern et al., 2005). Recently Braun et al. (2014) proposed that erosion-driven isostatic rebound should scale with the density of surface rocks: denser rocks, such as a granitic body intruded in sedimentary rocks, rebound and therefore are exhumed faster than the surrounding less dense rocks.

The rapid uplift of the Cordillera Blanca, the large volume of eroded

* Corresponding author at: Helmholtz-Zentrum Potsdam, GeoForschungsZentrum (GFZ) Potsdam, Potsdam, Germany.
E-mail addresses: audrey.margirier@gmail.com, audrey.margirier@gfz-potsdam.de (A. Margirier).

https://doi.org/10.1016/j.tecto.2018.02.009
Received 4 August 2017; Received in revised form 10 January 2018; Accepted 12 February 2018
Available online 14 February 2018

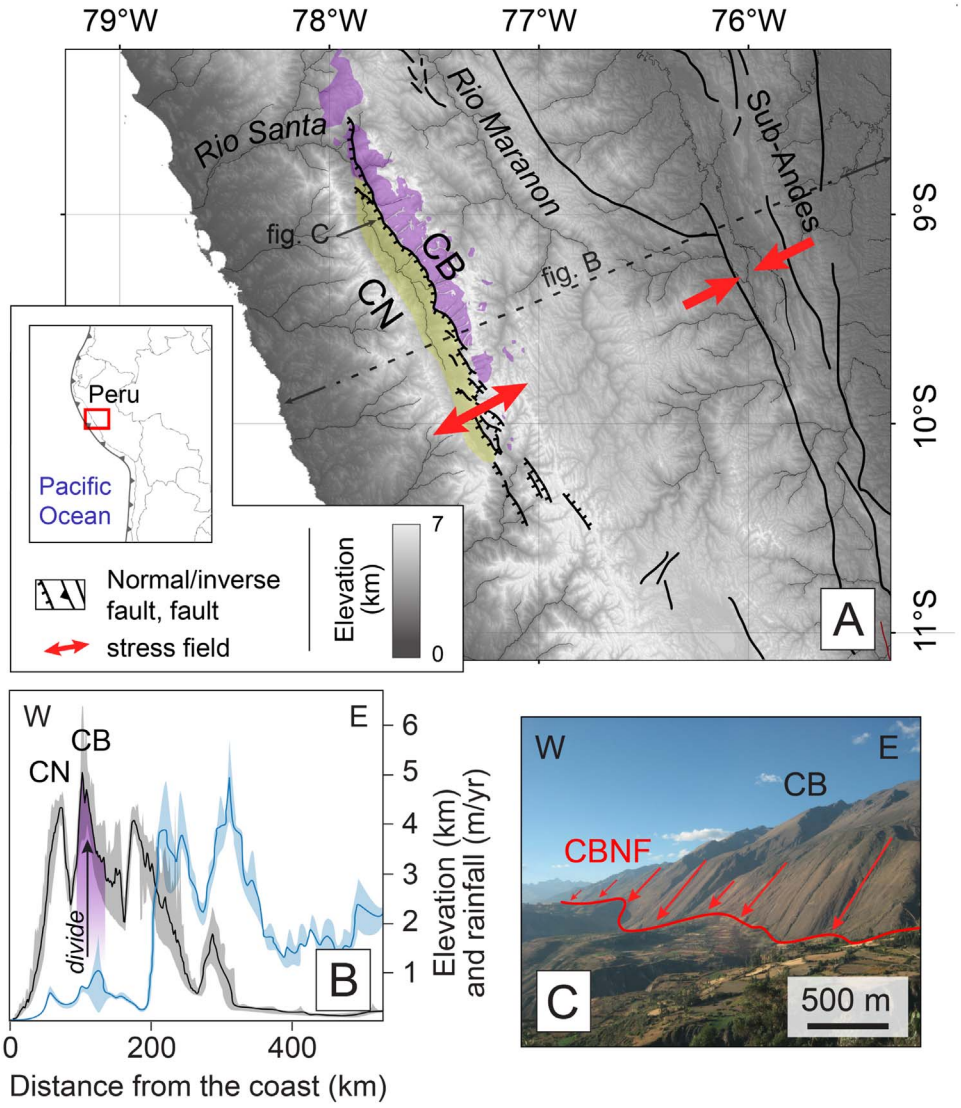

Fig. 1. A) Topographic map of the northern Peru showing active tectonic features (Neotectonic Open Database, neotec-opendata.com), location of the Cordillera Blanca (CB, the batholith is highlighted in purple), the Cordillera Negra (CN) and the Callejón de Huaylas (yellow). Inset shows map location within the South America. B) E-W cross-section of the Andes at the latitude of the Cordillera Blanca both the topography (black line) and the rainfall (blue line) are represented (modified from Bookhagen and Strecker, 2008). On the topographic cross-section the Cordillera Blanca batholith is represented in purple and a black arrow points the drainage divide location. C) Photograph of the CBNF showing the 1 km high triangular facets along the active fault scarp. (For interpretation of the references to color in this figure legend, the reader is referred to the web version of this article.)

rocks since the emplacement of the Cordillera Blanca batholith and its location in the footwall of an active normal fault in a compressive plate boundary, make the Cordillera Blanca the perfect place to question the nature and efficiency of potential feedbacks between erosion and uplift along the CBNF. The aim of this paper is thus (i) to test whether the increase of erosion rate suggested for the last 2 Ma in the Cordillera Blanca (Margirier et al., 2016) could be due to an increase of rock uplift rates since 2 Ma rather than a change of climate and/or erosion process and (ii) to quantify the importance of isostatic rebound associated with valley incision and erosion of denser rocks to explain the uplift of the Cordillera Blanca and to test the adequacy of a flexure-driven model in such a setting. To address this issue, we have attempted to model landscape evolution in the Cordillera Blanca using a landscape evolution model, in this case based on the FastScape algorithm (Braun and Willett, 2013).

2. Context

2.1. Geologic and climatic context

The Cordillera Blanca hosts the highest Peruvian summits with a cluster of 6000 m peaks (Fig. 1). It hosts a large 14–5 Ma granitic pluton (zircon U-Pb; Mukasa, 1984; Giovanni, 2007) emplaced at ~3 km depth into deformed Jurassic sediments (Margirier et al., 2016). The Cordillera batholith is elongated (150 × 15 km) and trends parallel to the Andean range (Fig. 1A). Based on apatite fission-tracks and (U-Th/He) dating several studies gave estimations of exhumation rates ranging between 1 and 2 mm/yr in the central part of the Cordillera Blanca for the last 3–4 Myr (Giovanni, 2007; Hodson, 2012; Margirier et al., 2015). This exhumation phase is likely associated to rock uplift and CBNF activity. On a shorter time scale (30–0 ka), the uplift rates have been constrained by ^{10}Be dating of scarps along the CBNF (Siame et al., 2006) and geomorphic features (moraines) displaced by the fault (Schwartz, 1988; Gérard et al., n.d.). The vertical slip rates decrease from north to south ranging from 5.1 ± 0.8 mm/yr to 0.6 ± 0.2 mm/yr (Schwartz, 1988; Siame et al., 2006; Margirier et al., 2017; Gérard et al., n.d.). Whereas the higher peaks in the Cordillera Blanca are located close to the CBNF and should therefore correspond to the region of maximum tectonic uplift, the drainage divide is located in the eastern part of the Cordillera Blanca, ~15 km away from the CBNF (Fig. 1B). The batholith is deeply incised by deep U-shaped valleys resulting from recent glacial erosion. Several other glacial landforms (moraines, roches moutonnées) are evidence of the large extension of the glaciations that shaped the Cordillera Blanca morphology (Farber et al., 2005). Today, the Cordillera Blanca summits form the Andean drainage divide (Wise and Noble, 2003) and act as an orographic barrier to moisture coming from the Amazon basin (Fig. 1B; Bookhagen and Strecker, 2008). Even if the most important orographic effect of the Andes is

controlled by the lower relief of the sub-Andes, the Cordillera Blanca high elevation prevents moisture from reaching the western flank of the Andes, resulting in wetter climatic conditions in the Cordillera Blanca (mean rainfall ~1.5 m/yr) than in the Cordillera Negra (mean rainfall ~0.5 m/yr), farther to the west (Bookhagen and Strecker, 2008).

The morphology of the Cordillera Negra is that of a 4500 m high plateau incised by 1–2 km deep valleys along its western flank (Fig. 1). The range hosts Cretaceous and Paleogene plutons (73–48 Ma; Beckinsale et al., 1985) intruded into Jurassic sediments. Neogene volcano-sedimentary deposits cap the Cordillera Negra (54–15 Ma Calipuy Formation; Cobbing et al., 1981). A regional surface uplift associated with the subduction geometry change and dynamic topography process has been evidenced in the Cordillera Negra from 15 Ma (Eakin et al., 2014; Margirier et al., 2015). Rare and discrete moraines, only seen above ~4200 m, indicate limited ice cover and resulting glacial erosion in the Cordillera Negra (Bonnot, 1984).

2.2. Paleogeography

Several studies have documented the Late Miocene paleogeography of the Cordillera Blanca region (Wise and Noble, 2003; Giovanni, 2007; Hoorn et al., 2010). Based on pollen analyses, Hoorn et al. (2010) constrained the elevation in the Cordillera Blanca region to be ~4 km in the Middle Miocene. However, at that time, the Cordillera Negra topography formed the main drainage divide (Wise and Noble, 2003). Based on the location, age and stratigraphy of volcanic deposits in the Callejón de Huaylas Basin that separates the two ranges, Wise and Noble (2003) and Giovanni (2007) suggested that a depression already existed between the Cordillera Blanca and the Cordillera Negra at the end of the Late Miocene. In addition, based on $\delta^{18}O$ analyses of paleolake deposits, Giovanni et al. (2010) showed that highest elevations in the Callejón de Huaylas Basin were attained in the latest Miocene. Little is known, however, about the topography of the Cordillera Blanca before the emplacement of the batholith.

3. Landscape evolution model: FastScape

3.1. Model

We used the FastScape algorithm (Braun and Willett, 2013) to solve the stream power law to predict landscape evolution following a set of tectonic forcing (uplift) and initial topography (geomorphic setting). Because of the optimum ordering of the nodes, the algorithm is implicit in time and computationally very efficient, requiring only O(n) operations where n is the number of points used to discretize the topography. Consequently, FastScape can be used repetitively, even if using a very high spatial discretization, to attempt to reproduce the main features of present-day topography and, using a simple 1D thermal model, predicted cooling ages (apatite fission-tracks and (U-Th/He) ages which can be related to erosion) in the hope of deducing a plausible first-order topographic and uplift history. To do this, we coupled FastScape to the neighborhood algorithm (NA) (Sambridge, 1999a; Sambridge, 1999b) to "invert" the thermochronological ages, the barometric constraints and the known, final topography in order to find the best-fitting values of several unknown parameters, including the erosion efficiency (K_f), the elastic thickness (T_e), the uplift rates (U_1) at several periods in the past and the temperature at the base of the model (T_{max}). Using NA, we first carried out a large number of FastScape runs with parameter values randomly selected between fixed limits. For each run the model predictions were compared to the data and a misfit function was estimated, which was used to select a new set of model parameters to be tested. This procedure was repeated several times until an optimum combination of parameter values was found and, more importantly, the shape of the misfit function could be mapped. This allows us to analyze and discuss the range of model parameters where the model prediction fits the observations, as well as the sensitivity of the model predictions to the model parameters.

3.2. Erosion and isostasy

To represent surface erosion, we solve the stream power law that is commonly used to parameterize bedrock incision by rivers in steep mountainous terrains:

$$\frac{\partial h}{\partial t} = U - K\, A^m\, S^n \tag{1}$$

where h is topographic height, t is time, U is uplift rate, A is drainage area and S is slope in the direction of water flow, taken here to be the steepest path between a point on the landscape and any among its eight neighbors. Parameters K, m and n are poorly constrained constants that mostly depend on lithology and climate. We will use m = 0.4, n = 1 and vary K around a mean value of $1.5 \times 10^{-5}\,\mathrm{m}^{1-2\mathrm{m}}\,\mathrm{yr}^{-1}$ (see Croissant and Braun (2014) for a discussion on the value of these parameters). We also assume that hillslopes are subject to mass transport at a rate that is simply linearly proportional to topographic slope. Assuming mass conservation, this leads to a law for the rate of change of topography on hillslopes that is proportional to the curvature of topography. Combining this with the stream power law leads to the following evolution equation for the surface topography:

$$\frac{\partial h}{\partial t} = U - K\, A^m\, S^n + K_D\left(\frac{\partial h^2}{\partial x^2} + \frac{\partial^2 h}{\partial y^2}\right) \tag{2}$$

where K_D is a transport coefficient or diffusivity. We will assume an arbitrary value of $K_D = 0.3\,\mathrm{m}^2/\mathrm{yr}$. We realize that using the stream power law and a simple diffusion-like representation of hillslope processes may seem inappropriate to model topographic evolution in a glaciated landscape. We justify our choice to use the stream power law by the fact that (i) no algorithm exists to solve the glacial erosion equations in an efficient manner that would allow for the type of inversion we have conducted here, (ii) we are interested in the effect of denser rocks erosion and the resulting isostatic rebound on the range-scale shape of the Cordillera Blanca and not in the details of the landform, and (iii) for both fluvial and glacial erosion processes, erosion rate is primarily controlled by slope and the geometry of a first order drainage system.

To account for the isostatic rebound associated with surface erosion, we also solve the following bi-harmonic equation representing the flexure of a thin elastic plate subject to surface loading/unloading:

$$D\left(\frac{\partial^4 w}{\partial x^4} + 2\,\frac{\partial^4 w}{\partial x^2 \partial x^2} + \frac{\partial^4 w}{\partial y^4}\right) = \Delta\,\rho g w + \rho_s g \Delta h \tag{3}$$

where w is the surface displacement associated with the isostatic adjustment of an increment in erosion Δh, D is flexural, ρ_s is the density of surface rocks and Δρ is the density contrast between asthenospheric density, ρ_a and surface rock density (Turcotte and Schubert, 2002).

A short word of explanation is necessary to understand how we have coupled Eqs. (2) and (3). As explained above, we assume that the imposed uplift rate does not contribute to the load applied to the thin elastic plate representing the lithosphere; only the eroded material does. This means that we can rewrite Eq. (2) in the following form:

$$\frac{\partial h}{\partial t} = U - F(e)$$

where e is erosion rate:

$$e = KA^m S^n - K_D\left(\frac{\partial^2 h}{\partial x^2} + \frac{\partial^2 h}{\partial y^2}\right)$$

and F(e) is the rate of isostatic response to this erosion rate. U is the uplift rate that would result in the absence of erosion. We can make this equation more readily understandable, if we assume local isostasy, in which case, it becomes:

$$\frac{\partial h}{\partial t} = U - \left(1 - \frac{\rho_s}{\rho_a}\right)e$$

We see that when erosion rate is nil, the rate of surface uplift is U but that the steady state erosion rate, e_{ss}, i.e. corresponding to $\partial h/\partial t = 0$:

$$e_{ss} = U/\left(1 - \frac{\rho_s}{\rho_a}\right)$$

is larger than U. Consequently, during a numerical experiment, we expect to see the erosion rate progressively increase to values that can reach 5–6 times the imposed uplift rate. Flexure should dampen this progressive increase of the erosion rate as a function of time.

3.3. Age predictions

As stated earlier, we will constrain our inversion by testing model predictions against observed cooling ages obtained for a series of samples collected in the Cordillera Blanca (Montario, 2001; Giovanni, 2007; Hodson, 2012; Margirier et al., 2015). At each point of the model where we wish to predict a cooling age, we solve the 1D heat transport equation by conduction and advection:

$$\frac{\partial T}{\partial t} + \mathrm{v}\frac{\partial T}{\partial z} = \kappa \frac{\partial^2 T}{\partial z^2} \quad (6)$$

where κ is thermal diffusivity and v is the erosion rate predicted by the landscape evolution model. We neglect the effect of radiogenic heat production and assume that the top and base of the crust/lithosphere are held at constant temperature: $T(z = 0) = 0$ and $T(z = L) = TL$. The thermal history obtained by solving this equation through time is then used to compute cooling ages by using standard methods developed to simulate the annealing of fission tracks and the diffusion of He in apatite (Braun et al., 2006).

The thermochronological dataset consists of apatite fission-track (AFT) ages and (U-Th)/He (AHe) mean ages (Montario, 2001; Giovanni, 2007; Hodson, 2012; Margirier et al., 2015). The AFT and AHe thermochronological systems record the cooling histories of rocks below 120 °C and 80 °C, respectively; at a given location subject to steady exhumation, AFT age should be older than AHe age. For our inversions we exclude AFT ages that are older than the age of the emplacement of the Cordillera Blanca batholith (~7 Ma; Mukasa, 1984; Giovanni, 2007) and the AHe ages that are older than AFT age for a same sample. Indeed, the AHe ages are scattered, raising the question of their reliability (Margirier et al., 2015).

The misfit function used to guide the inversion procedure is defined by:

$$\mu = \frac{1}{N}\sqrt{\sum \frac{(Age_o - Age_p)^2}{\partial \Delta Age^2}} + \frac{|Hmax_o - Hmax_p|}{\Delta Hmax} + \frac{|Vmax_o - Vmax_p|}{\Delta Vmax} \quad (7)$$

where N is the number of thermochronological ages, Age_{oi} and Age_{pi} the observed and predicted ages and ΔAge_i the uncertainty on the observed ages. $Hmax_o$ and $Hmax_p$ are the observed (present-day) and predicted maximum topography of the Cordillera Blanca (6600 m) and ΔHmax its regional variability (200 m). $Vmax_o$ and $Vmax_p$ are the observed (present-day) and total exhumed volume of the Cordillera Blanca (1×10^{13} m^3), which we derive from amphibole barometry data (Margirier et al., 2016), and ΔVmax its assumed uncertainty (5×10^{12} m^3).

3.4. Parameterization

For each inversion, we ran 15,000 models; during the first iteration, we sampled 3000 models to explore the parameter space, then we performed 15 iterations of 800 models with 400 cells resampled. The

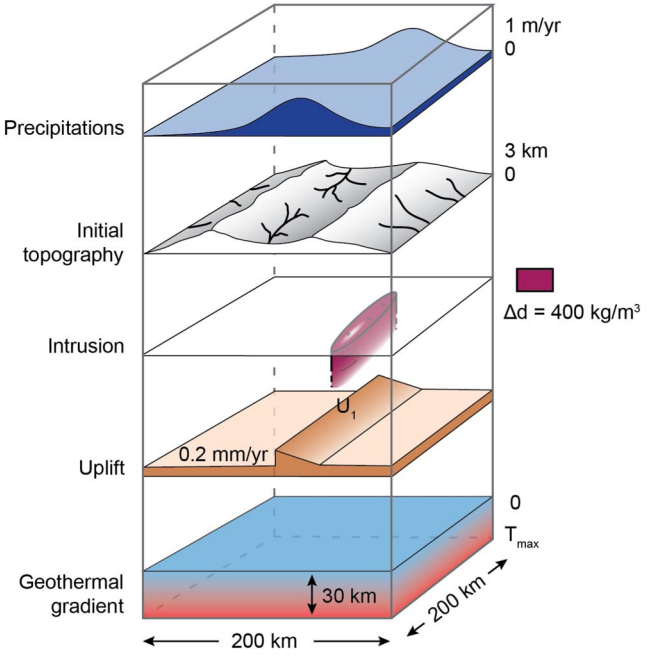

Fig. 2. Parameterization of the models.

runs were performed on a 200 × 200 km square domain (Fig. 2), discretized by 500 × 500 regularly space nodes. All model runs last 7 Ma, which is approximately equivalent to the age of the Cordillera batholith emplacement (see geochronological data compilation in Margirier et al., 2016). We chose to take the geological ages as references for the modelisations, thus the model runs begin at 7 Ma and end at 0 Ma. We fixed the time step length to 1 ka (other model parameters are detailed in the Table A1). We used an arbitrary initial topography including both a "proto Cordillera Negra" (3500 m) and, for inversions 1b and 2, a "proto Cordillera Blanca" (3000 m), following estimates from Wise and Noble (2003) and Hoorn et al. (2010). We imposed a uniform precipitation rate of ~0.5 m/yr in the Cordillera Negra and ~1.0 m/yr in the Cordillera Blanca in accordance with present-day estimates from Bookhagen and Strecker (2008). According to the Cordillera Blanca batholith lithology and shape (granite/granodiorite with a typical density ~2800 kg/m^3; Petford and Atherton, 1992; Sharma, 1997) and the nature of the surroundings sedimentary rocks (alternating sandstone and marl with sporadic limestone with an estimated density ~2400 kg/m^3; Bonnot, 1984; Sharma, 1997), we included a 150 × 20 km ellipsoidal intrusion that is characterized by an anomalously high density (400 kg/m^3 heavier than the surrounding rocks). The top of the intrusion is initially at 1.5 km beneath sea level (~3 km depth). This is constrained by amphibole barometry data obtained from the roof of the Cordillera Blanca batholith (Margirier et al., 2016). We fixed a regional uplift rate $U_0 = 0.2$ mm/yr in agreement with the thermal history provided by Margirier et al. (2015) for the Cordillera Negra. In addition to the widespread uplift (U_0) we simulated the presence of an active fault by imposing a steep gradient in vertical displacement rate along a north-south boundary located a distance of 100 km from the left side of the model (Fig. 2). Along the boundary the uplift rate is equal to U_1 and it decreases linearly to reach a value of 0 at 25 km away from the boundary. The uplift history along this boundary is divided into 3 successive episodes based on observations concerning the initiation of the CNBF and an apparent increase in erosion rate evidenced by Margirier et al. (2016). From 7 to 5.4 Ma (before the CBNF initiation) the uplift rate (U_1) is equal to 0; between 5.4 and 2 Ma, the uplift rate is constant (and equal to U_1); between 2 Ma and the present, the uplift rate is increased by a factor f_{U1}. Perez-Gussinye et al. (2009) estimated elastic thickness (T_e) to be in the range (0 − 10) km, which are relatively low values for continental regions; we use a value

of 3 km in inversions where the elastic thickness is fixed. The four parameters that we want to constrain by inversion of the thermochronological ages and the range-scale present-day topography and eroded volume in our inversions, are the erosion efficiency (K_f), the mean uplift rate (U_1), the magnitude of the recent increase of uplift rate in the Cordillera Blanca (f_{U1}), the temperature at the base of the model (T_{max}) and, in a third set of inversions, the elastic thickness of the lithosphere (T_e).

4. Results

4.1. Role of tectonics, erosion and initial topography

Here we aim to test (i) if the increase of erosion rate suggested for the last 2 Ma in the Cordillera Blanca (Margirier et al., 2016) could be due to an increase in uplift rates since 2 Ma rather than a change of climate and/or erosion process (glacial erosion vs fluvial erosion) and (ii) the role of initial topography in the present day Cordillera Blanca drainage divide location. In these inversions, the four parameters that we wanted to constrain by inversion of the thermochronological ages, the total exhumation and the range-scale present-day topography are the erosion efficiency (K_f), the mean uplift rate (U_1), the magnitude of the recent increase of uplift rate in the Cordillera Blanca (f_{U1}) and the temperature at the base of the model (T_{max}).

We performed two inversions, one without an initial topography in the Cordillera Blanca and a second one with a 'proto Cordillera Blanca', in order to evaluate the paleogeography and inherited drainage network influence on the location of the present day drainage divide in the Cordillera Blanca.

4.1.1. Inversion 1a (without a 'proto Cordillera Blanca')

Fig. 3 presents the results of inversion 1a (without a 'proto Cordillera Blanca') as values of the misfit function, μ, displayed in parameter space. In each of the two panels, each dot represents a single model run and the color scale refers to the value of the misfit of the model (from blue for high misfit value or poor fit to the data, to red for low misfit value or good fit to the data). In each of the panels, the red star indicates the position of the best-fitting model in parameter space.

The mean uplift rate (U_1), the amplitude of its recent increase (f_{U1}) and the erodibility (K_f) are all well constrained by the thermochronological data (Fig. 3) although a trade-off exists (as shown in Fig. 3B) between U_1 and f_{U1}. These two parameters are clearly correlated with higher mean uplift rate requiring a smaller recent increase in uplift rate and vice-versa. The arcuate shape of the region of minimum misfit in Fig. 3B can also be interpreted by stating that the product $U_1 \times f_{U1}$ (or in other words the uplift rate between 2 and 0 Ma) is very well constrained by the data at a value of approximately 1.8 mm/yr (the best fitting parameters are indicated by a red star on Fig. 3A and B). The temperature at the base of the model is not as well constrained (Fig. 3A) although values between 650 and 850 °C yield the lowest misfit values. These values should be interpreted as suggesting best fitting surface geothermal gradient values of 21 to 28 °C/km. The inversion results suggest that the data is best explained by values of $K_f = 1.9 \times 10^{-5}\,m^{1-2m}\,yr^{-1}$, $U_1 = 0.80$ mm/yr, $f_{U1} = 1.8$ and $T_{max} = 677$ °C. The set of the good fitting value of f_{U1} (misfit < 0.6) indicates that a substantial increase in erosion rate in the recent past is necessary to explain the age dataset and the total exhumation. The best value for the basal temperature ($T_{max} = 677$ °C) corresponds to a geothermal gradient of ~23 °C/km, which is consistent with Henry and Pollack (1988) terrestrial heat flow measurements.

The misfit is 0.53 for the best fitting parameters model, suggesting that the model can reproduce the data (present-day topography, total exhumation and thermochronological ages, Fig. 3). In addition, the thickness of rock eroded in the model after 7 Ma reproduces the total eroded volume we fixed to correspond with field observations and granite emplacement depth obtained by Margirier et al. (2016). However, the apatite fission track ages are not well reproduced by the best fitting parameters model, the apatite (U-Th)/He ages predicted by the

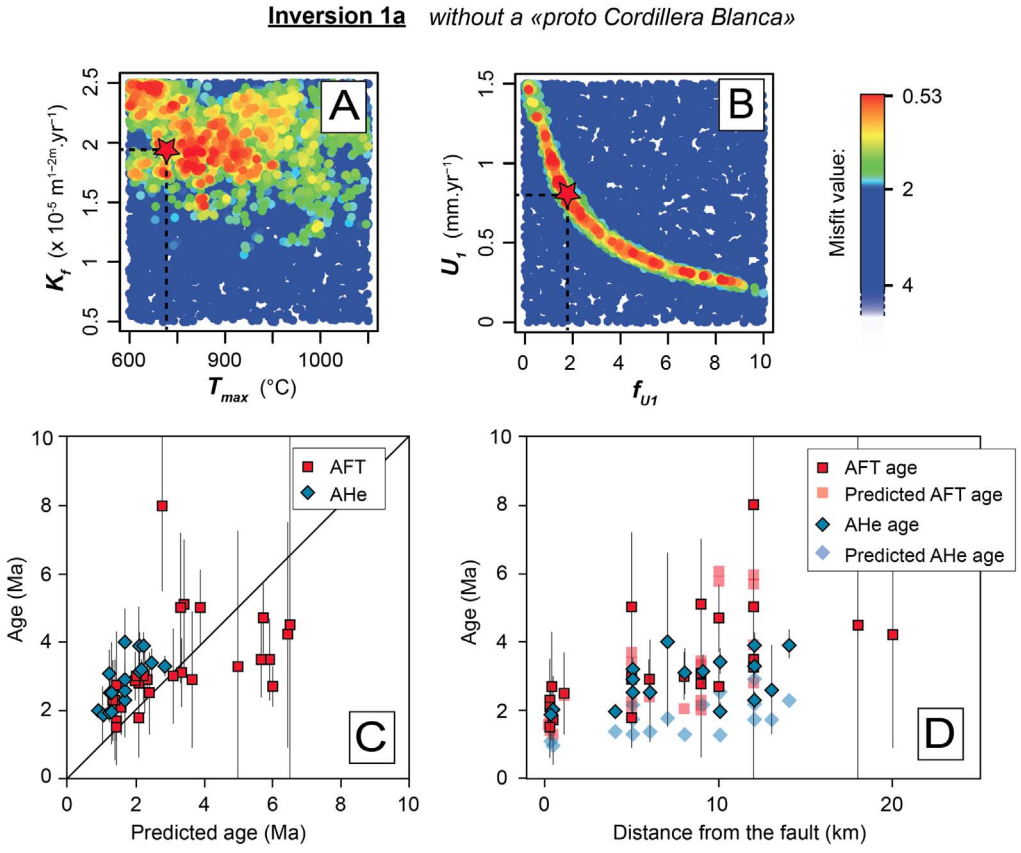

Fig. 3. Results of the NA inversion 1a. A, B) Scatter plots colored by likelihood values for erosion efficiency (K_f), basal temperature (T_{max}), uplift rate (U_1) and factor of uplift rate increase for the last 2 Ma (f_{U1}). The most likelihood model is indicated with a red star. C) Comparison between observed ages and synthetic ages predicted by the best-fit model for apatite fission-track ages and apatite (U-Th)/He ages. D) Observed ages and synthetic ages vs. distance to the Cordillera Blanca normal fault. (For interpretation of the references to color in this figure legend, the reader is referred to the web version of this article.)

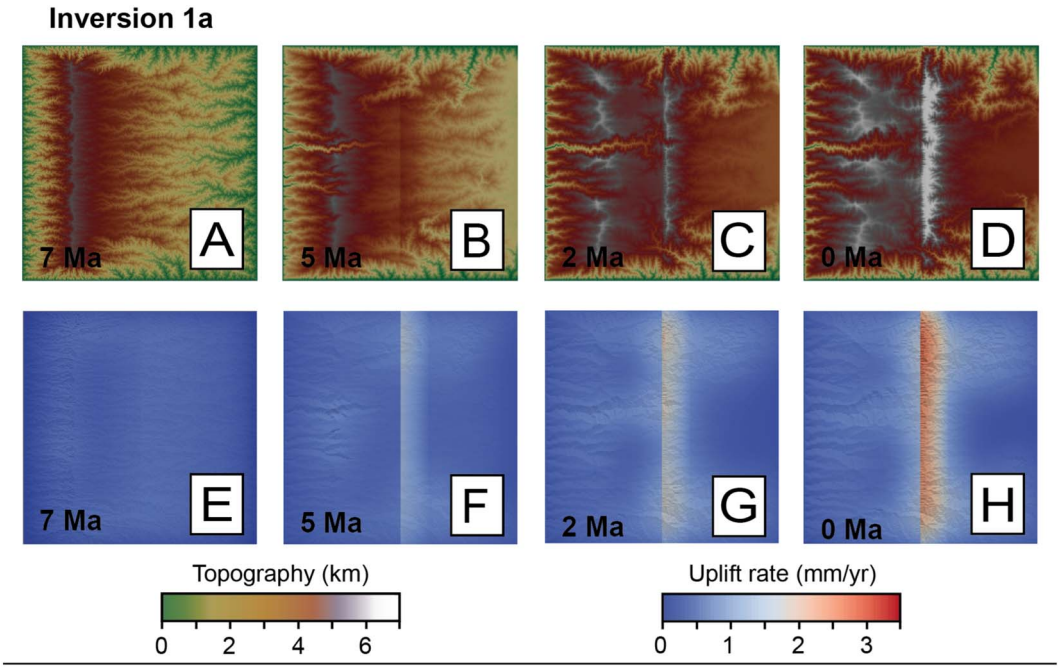

Fig. 4. Evolution of the topography and rock uplift rate for the best fitting parameter model of inversion 1a. A–D) Topography, E–H) Rock uplift rate.

model are too young (Fig. 3C, D). Moreover, the best fitting parameters model does not reproduce all characteristic features of the present-day Cordillera Blanca topography. Notably, the drainage divide of the predicted topography is located close to the CBNF, which is not the case in the Cordillera Blanca (Figs. 1, 4).

4.1.2. Inversion 1b (with a 'proto Cordillera Blanca')

We performed a second inversion (inversion 1b) using the same constraints as for inversion 1a but with a finite initial topography in the Cordillera Blanca (see initial topography on Fig. 2). Fig. 5A, B presents the results of the inversion as values of the misfit function, μ, displayed in parameter space. The misfit is 0.44 for the best fitting parameters model, indicating that the model can reproduce the present-day topography, total exhumation and thermochronological ages (Fig. 5C, D) as well as the best model of inversion 1a.

The mean uplift rate (U_1), the amplitude of its recent increase (f_{U1}) and the erosion efficiency (K_f) are all well constrained by our data. Similarly to inversion 1a, U_1 and f_{U1} are correlated with higher mean uplift rate requiring a smaller recent increase in uplift rate and vice-versa. The arcuate shape of the region of minimum misfit in Fig. 5B can also be interpreted by stating that the product $U_1 \times f_{U1}$ is very well constrained by the data at a value of approximately 1.0 mm/yr. The temperature at the base of the model (T_{max}) is not as well constrained (Fig. 5A, B) although values between 850 and 1050 °C yield the lowest misfit values. These values should be interpreted as suggesting best fitting surface geothermal gradient values of 28 to 35 °C/km. The inversion result suggests that the data is best explained by values of $K_f = 1.3 \times 10^{-5}\,m^{1-2m}\,yr^{-1}$, $U_1 = 0.52$ mm/yr, $f_{U1} = 2.0$ mm/yr and $T_{max} = 945$ °C. The best value for the basal temperature ($T_{max} = 945$ °C) corresponds to a geothermal gradient of ~32 °C/km.

Fig. 6 presents the topographic evolution and the uplift rates predicted in the Cordillera Blanca using the best fitting parameters. Predicted uplift rates obtained at the end of the model are higher than the imposed uplift rate due to isostasy (Figs. 5, 6). Considering the low elastic thickness of the lithosphere used in this model ($T_e = 3$ km), according to existing estimate of the elastic thickness of the lithosphere in the Cordillera Blanca region (0–10 km; Perez-Gussinye et al., 2009), the flexural rebound is substantial. As explained in the method section, if we chose to ignore the flexural rebound due to erosion, the uplift rates would correspond to the vertical displacement (i.e. tectonic forcing) imposed on the fault ($U_1 = 0.52$ mm/yr and $U_1 \times f_{U1} = 1.0$ mm/yr) but if we consider the flexural rebound associated with the erosion, the uplift rates significantly increase with time (up to ~2 mm/yr; Fig. 6). The predicted uplift rates at the end of the model are consistent with the Quaternary vertical slip rates on the CBNF ranging from 5.1 ± 0.8 mm/yr to 0.6 ± 0.2 mm/yr (Schwartz, 1988; Siame et al., 2006; Margirier et al., 2017) and with ^{10}Be catchment-wide erosion rates in the Cordillera Blanca (mean of 0.7 mm/yr; Hodson, 2012).

4.1.3. Comparison between the results of the two inversions

Best fitting parameters for inversion 1b are in the same order of magnitude as for inversion 1a. However, we obtained a larger value for the product $U_1 \times f_{U1}$ for the inversion 1a, indicating larger total uplift in the Cordillera Blanca since 5.4 Ma. This can be easily explained by the lower initial elevation in the inversion without an initial topography; thus to reach the present day elevation of the Cordillera Blanca, the total uplift has to be larger.

The most striking difference between these two inversions is that without a 'proto Cordillera Blanca' (inversion 1a), even if the predicted elevations are well correlated with the observed topographic bulge in the Cordillera Blanca, the model still does not reproduce the present-day location of the main drainage divide (Fig. 7). Notably, for the model without initial relief in the Cordillera Blanca the drainage divide is located close to the CBNF, which is not the case for the present-day topography. The existence of an early relief, the 'proto Cordillera Blanca', probably controls the early drainage network and localizes the drainage divide farther east in the present day Cordillera Blanca. Our results suggest that the presence of an initial relief is needed to localize the drainage divide at its present position (eastern part of the Cordillera Blanca), although we cannot preclude a different scenario.

4.2. Role of the granite

In the Cordillera Blanca the granite reached the surface and starts to be eroded at ~3 Ma (Bonnot, 1984). This enables us to explore the influence of eroding denser rocks on the evolution of topography and uplift rates on a Ma time scale. We performed additional inversions (2a and 2b) of the topography, the total exhumation and

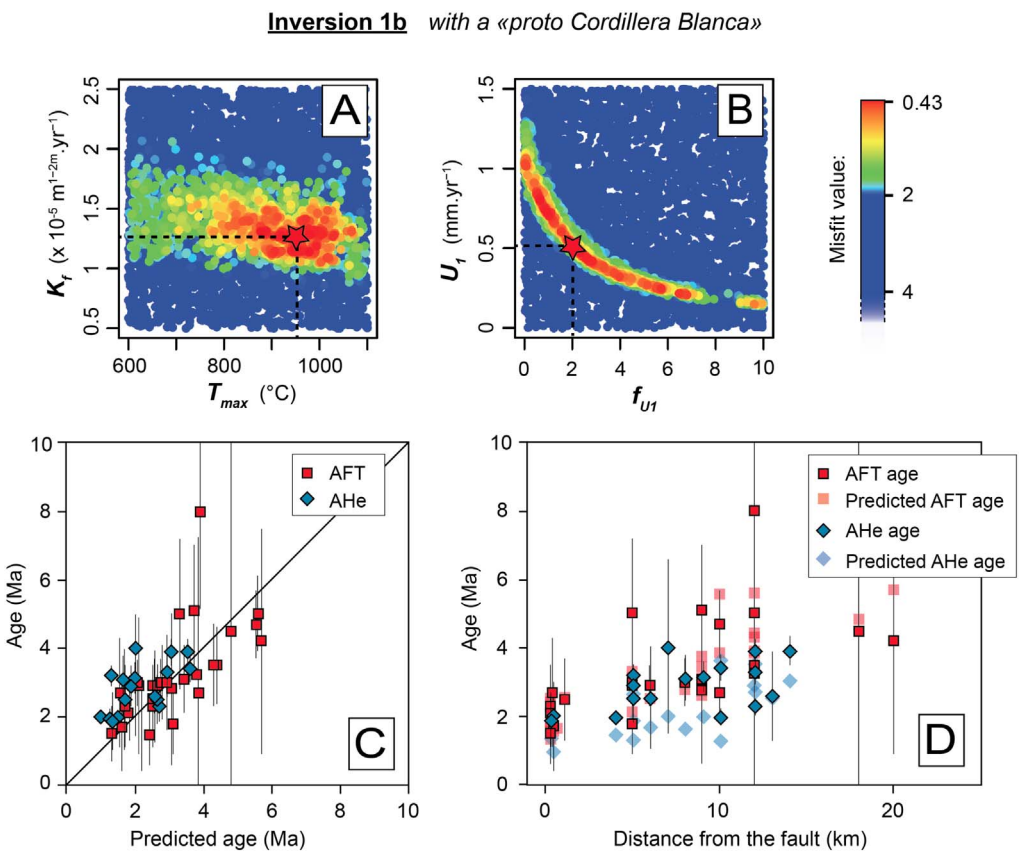

Fig. 5. Results of the NA inversion 1b. A, B) Scatter plots colored by likelihood values for erosion efficiency (K_f), basal temperature (T_{max}), uplift rate (U_1) and factor of uplift rate increase for the last 2 Ma (f_{U1}). The most likelihood model is indicated with a red star. C) Comparison between observed ages and synthetic ages predicted by the best-fit model for apatite fission-track ages and apatite (U-Th)/He ages. D) Observed ages and synthetic ages vs. distance to the Cordillera Blanca normal fault. (For interpretation of the references to color in this figure legend, the reader is referred to the web version of this article.)

thermochronological ages to assess the role of the intrusion in the recent increase of uplift rates in the Cordillera Blanca and in high topography building. In these two inversions the initial topography includes a proto Cordillera Blanca and we fixed $f_{U1} = 1$ (no uplift increase after 2 Ma) in order to test if the increase of the uplift rate due to the batholith erosion could explain by itself the increase of erosion rates observed by (Margirier et al., 2016). The inversion 2a didn't include an intrusion. Then, the inversion 2b included an intrusion that is characterized by an anomalously high density (400 kg/m^3 heavier than the surrounding rocks). In these inversions the parameters that we aimed to constrain were K_f, T_e, U_1, and T_{max}. Fig. 8 presents the results of the inversions 2a and 2b as values of the misfit function, μ, displayed in parameter space.

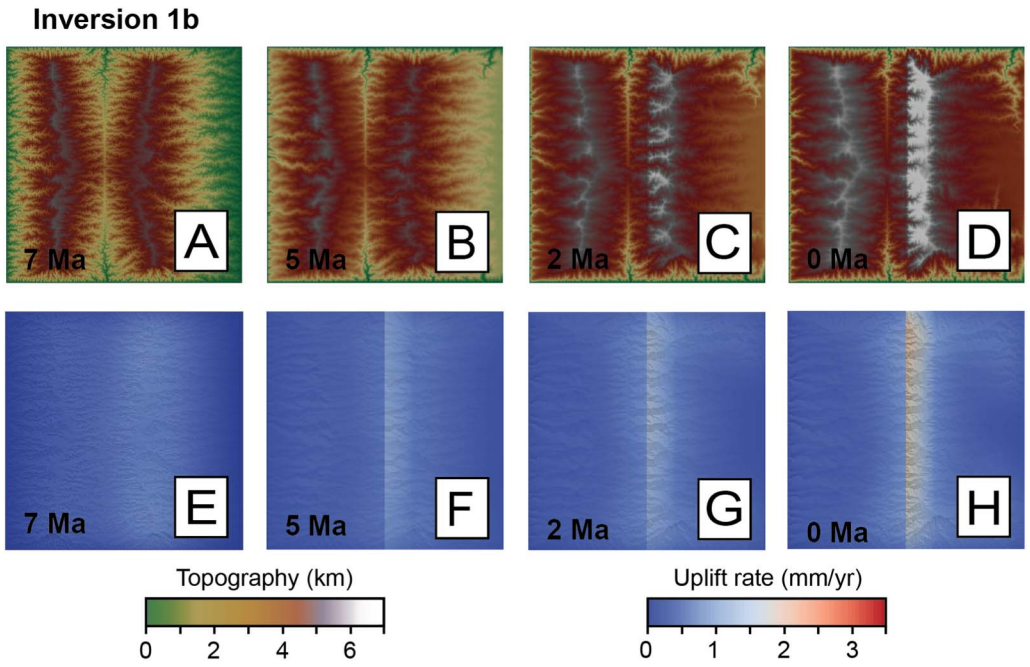

Fig. 6. Evolution of the topography and rock uplift rate for the best fitting parameter model of inversion 1b. A–D) Predicted topography, E–H) Map of the predicted rock uplift rate.

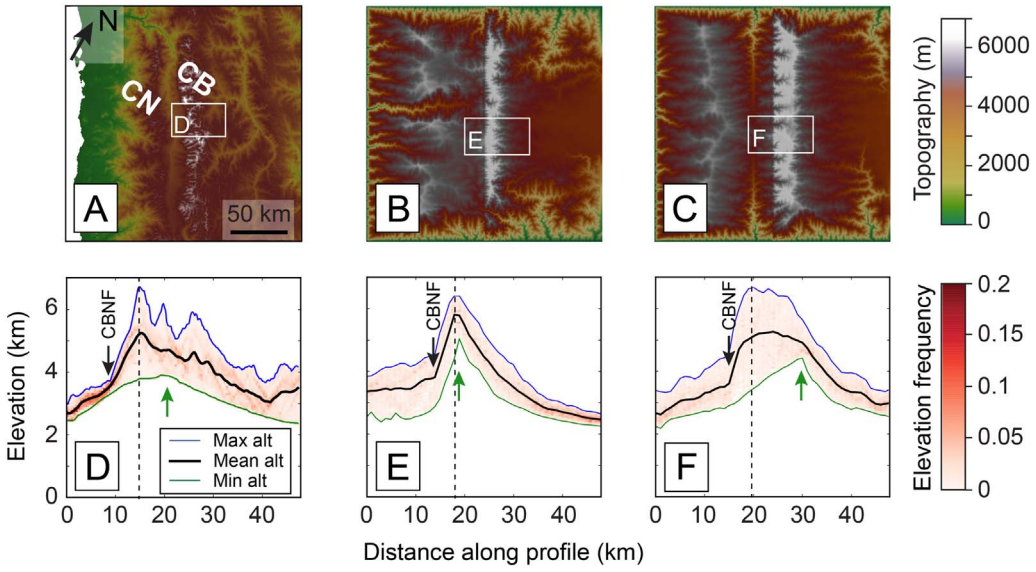

Fig. 7. DEM and swath profiles through the Cordillera Blanca region and modeled topography. A) DEM of the Cordillera Blanca region. B) DEM of the best model of inversion 1a, which involves a fault, a granitic batholith, a flexural rebound and a "proto" Cordillera Negra. C) DEM of the best model of inversion 1b with both a 'proto Cordillera Negra' and a 'proto Cordillera Blanca'. D–F) Swath profiles through the Cordillera Blanca and from the two models showing elevation (mean, maximum and minimum), the drainage divide position (green arrow), the CBNF location (black arrow) and the maximum elevation (vertical dot line). (For interpretation of the references to color in this figure legend, the reader is referred to the web version of this article.)

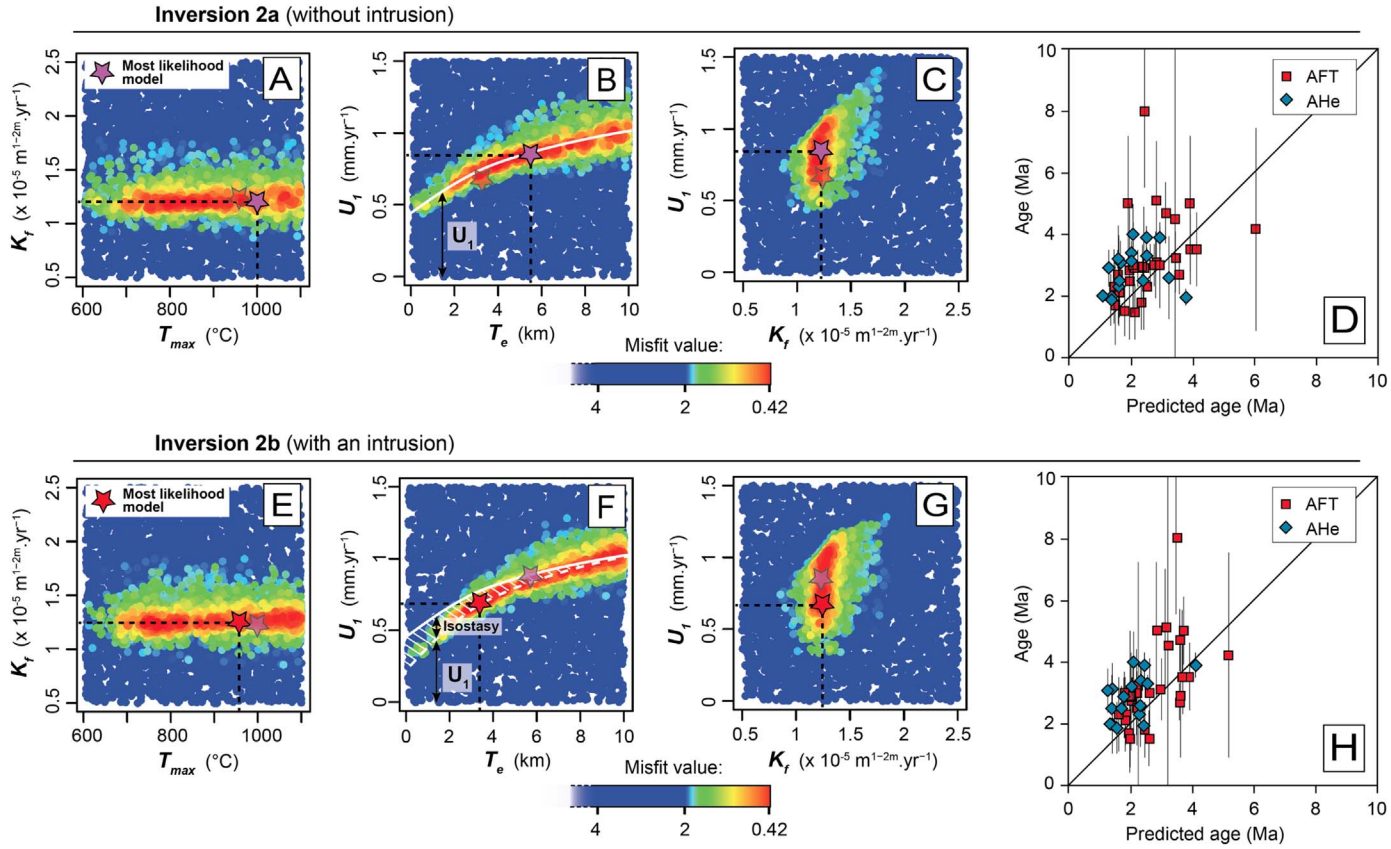

Fig. 8. Results of the NA inversions 2a and 2b as scatter plots colored by likelihood values (from blue for high misfit value or poor fit to the data, to red for low misfit value or good fit to the data) for erosion efficiency (K_f), basal temperature (T_{max}), uplift rate (U_1) and elastic thickness of the crust (T_e). The most likelihood models are indicated with purple stars (inversion 2a) and red stars (inversion 2b). A–C) Scatter plots and D) comparison between observed thermochronological ages and synthetic ages predicted by the best-fit model for the inversion 2a (without intrusion). E–G) Scatter plots for inversion 2b (with an intrusion). H) Comparison between observed thermochronological ages and synthetic ages predicted by the best-fit model for the inversion 2b. (For interpretation of the references to color in this figure legend, the reader is referred to the web version of this article.)

4.2.1. Inversion 2a (without contrasting density intrusion)

The misfit of inversion 2a is 0.42 for the best fitting parameters model, indicating that the model can reproduce the present-day topography, total exhumation and thermochronological ages (Fig. 8D). In this inversion without intrusion, the mean uplift rate (U_1) and the erodability (K_f) are also well constrained whereas the temperature at the base of the model (T_{max}) and the elastic thickness of the crust (T_e) are not as well constrained (Fig. 8A, B, C), although values between 750 and 1050 °C and 3 and 7 km respectively yield the lowest misfit values. These values should be interpreted as suggesting best fitting surface geothermal gradient values of 25 to 35 °C/km. The data is best explained by very similar values of $K_f = 1.2 \times 10^{-5}\,m^{1-2m}.yr^{-1}$, $T_e = 5.6$ km, $U_1 = 0.86$ mm/yr, and $T_{max} = 1001$ °C. The best value for the basal temperature ($T_{max} = 1001$ °C) corresponds to a geothermal

gradient of ~33 °C/km.

4.2.2. Inversion 2b (with contrasting density intrusion)

The lowest misfit is 0.42 for inversion 2b, suggesting that the model can also reproduce the present-day topography, total exhumation and thermochronological ages (Fig. 8). In this inversion that includes a dense intrusion, the mean uplift rate (U_1) and the erosion efficiency (K_f) are all well constrained (Fig. 8E, F, G). The temperature at the base of the model (T_{max}) and the elastic thickness of the crust (T_e) are not as well constrained although values between 750 and 1050 °C and 3 and 5 km respectively yield the lowest misfit values (Fig. 8E, F). These T_{max} values should be interpreted as suggesting best fitting surface geothermal gradient values of 25 to 35 °C/km. U_1 and T_e are clearly correlated with smaller elastic thickness of the crust requiring smaller uplift rate and vice-versa. The inversion result suggests that the data is best explained by values of $K_f = 1.2 \times 10^{-5}\,m^{1-2m}\,yr^{-1}$, $T_e = 3.3$ km, $U_1 = 0.69$ mm/yr, and $T_{max} = 954$ °C. The best value for the basal temperature ($T_{max} = 954$ °C) corresponds to a geothermal gradient of ~32 °C/km.

4.2.3. Comparison between the results of the two inversions

For these two inversions the predicted elevations are well correlated with the observed topographic bulge in the Cordillera Blanca. The models also reproduce the present-day location of the main drainage divide and the thermochronological ages (Fig. 8D, H). The best fitting K_f, T_e and T_{max} are not significantly different for the best models 2a and 2b. For both inversions the best fitting T_e (~4 km) is consistent with Perez-Gussinye et al. (2009) predictions at a larger scale. However, the good fitting values of U_1 (misfit < 0.6) are significantly smaller for the inversion 2b (with an intrusion) than 2a, especially if the elastic thickness decreases below 4 km (Fig. 7). Fig. 9 shows the predicted topography and uplift rate at the end of the best fitting parameters models for inversion 2a (without intrusion) and 2b (with an intrusion). Taking isostasy into account, the two best fitting parameters models reach a maximum uplift rate of 1.7 mm/yr at the end of the run. The maximum uplift rates obtained from our models at the end of the runs are similar to the Quaternary vertical slip rates documented along the CBNF and are in the same order of magnitude than ^{10}Be catchment-wide erosion rates obtained in the Cordillera Blanca (Schwartz, 1988; Siame et al., 2006; Hodson, 2012; Margirier et al., 2017). Since the predicted maximum uplift rates are similar at the end of the two models which take isostasy into account (1.7 mm/yr; Fig. 9C, D), the difference between the good fitting U_1 values (misfit < 0.6) can be explained by the more important contribution of isostasy for the model including a dense intrusion.

5. Discussion

5.1. Paleogeography

The substantial surface uplift and resulting erosion in the Cordillera Blanca make it difficult to study the paleogeography in this area based on remnants geomorphological features. However, the drainage network geometry and the drainage divide location provide information on the topography of the Cordillera Blanca in the past and its evolution. Notably, the Cordillera Blanca drainage divide is located in the eastern part of the range whereas both the higher peaks and higher uplift rates are located in the western flank of the Cordillera Blanca (Margirier et al., 2016). But the precipitation gradient, with higher mean precipitation on the eastern flank of the Cordillera Blanca, should favor the location of the drainage divide further west. Our results suggest that the location of the drainage divide in the eastern part of the Cordillera Blanca is controlled by an initial topography in the Cordillera Blanca area and an inherited drainage network. Based on these results we propose that a proto-Cordillera Blanca existed before the CBNF initiation ~5 Myr ago. The presence of such a relief is in agreement with Giovanni et al. (2010) and Wise and Noble (2003), which already proposed that the Callejón de Huaylas was a topographic depression

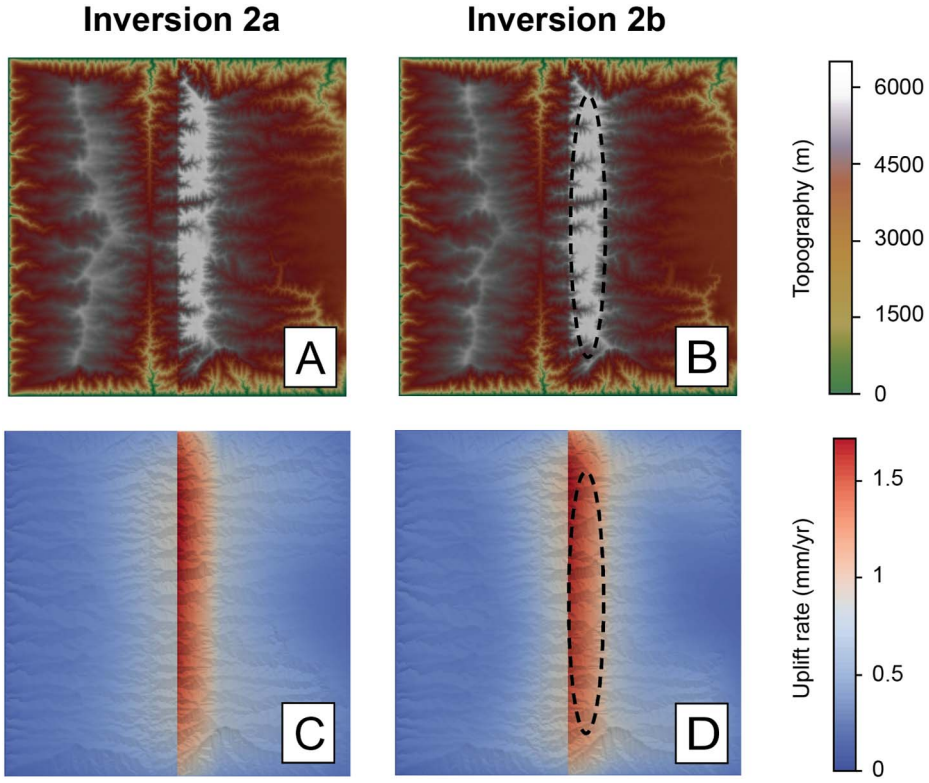

Fig. 9. Map of the topography at the end of the model A) without granite and B) with a dense granite. Map of the uplift rates at the end of the model C) without granite and D) with a dense granite. The oval dotted line indicates the location of the granite.

during the Late Miocene. Wise and Noble (2003) suggested that at that time, before the Cordillera Blanca exhumation, the Cordillera Negra corresponded to the drainage divide. However, the presence of a proto-Cordillera Blanca calls into question the position of the Andean drainage divide during the Miocene.

5.2. The Cordillera Blanca uplift: role of granite erosion and flexural rebound

Our results show a difference in imposed uplift rates for the best fitting models of the inversions 2a and 2b that do not or do include a granite (U_1 = 0.86 mm/yr versus U_1 = 0.69 mm/yr; Fig. 8). In addition, our models do not take into account the presence of the CBNF for the isostatic response calculation despite the existence of a 200 km-long crustal fault (Dalmayrac and Molnar, 1981; McNulty and Farber, 2002). If, to reflect the regional geology, we had used a broken plate approximation to calculate the isostasy contribution to uplift and erosion, the isostatic response would, potentially, have been more important. In addition, even when considering the best fitting value for T_e the role of the granite seems to be small; if we consider the range of acceptable values for T_e, we notice that smaller values of T_e would increase the importance of isostasy, which, in turn, would require smaller valued of imposed uplift, U_1 (Fig. 8E). For example, if we consider the best fitting models or the models involving a 3 km elastic thickness which also show low misfit values, the isostasy contributes c.a. 20% of the total rock uplift (Fig. 8B, F). Considering that for the best fitting parameters model of the inversion 2b, the granite reaches the surface approximately 3 Ma before the end of the model run, our results indicate that the isostatic effect of eroding a denser rock mass is not negligible even on a < 5 Ma time scale. Finally, we note that the inversion that includes a denser granite (inversion 2b) converges toward smaller values for the imposed uplift rate, U_1, than the inversion which doesn't include an intrusion (inversion 2a) implying that erosion of the Cordillera Blanca dense intrusion may substantially contribute to the present-day higher uplift rates as proposed by Braun et al. (2014).

Interestingly, our results suggest that the recent increase in exhumation rate documented by Margirier et al. (2016) might not be the result of a change in tectonic since 2 Ma or climate forcing, but the result of the progressive flexural isostatic response of the area to erosion. At the onset of uplift, slopes are relatively low, erosion is limited to the sides of the uplifting region and the weight of uplifted material acts as a negative feedback to further uplift; as the uplifting region becomes affected by surface processes (fluvial erosion in our model, but more likely glacial erosion in the Cordillera Blanca) the resulting erosional unloading reduces the negative feedback and uplift and erosion rates increase until a steady-state situation is reached between uplift, erosion and isostasy. The time scale over which this steady-state balance is reached must be of the order of a few million years, at least (Whipple and Meade, 2006).

From the time when the Cordillera Blanca summits reached high elevation, the Cordillera Blanca itself has acted as an orographic barrier for moisture carried from the Amazon basin (Montgomery et al., 2001; Bookhagen and Strecker, 2008). The induced rain shadow included in our model prevents erosion of the Cordillera Negra, and results in higher erosion rates in the Cordillera Blanca (i.e. Montgomery and Brandon, 2002) in the recent past. It is also likely that Quaternary glaciations (~1.5–0 Ma; Farber et al., 2005; Smith et al., 2005) have increased erosion rates through the formation of deeply incised U-shaped valleys, as evidenced by Montgomery (2002) for the Olympic Mountains on the Pacific coast of the North America and suggested by Margirier et al. (2016) for the Cordillera Blanca. Finally, the recent glacial retreat (since ~21 ka; Seltzer et al., 2002; Farber et al., 2005; Smith et al., 2005) could have induced a flexural rebound that both increased uplift rates in the Cordillera Blanca and slip-rates on the CBNF (e.g., Hetzel and Hampel, 2005; Hampel et al., 2007).

5.3. Models for the CBNF

Two models have been proposed to explained extension on the CBNF. Dalmayrac and Molnar (1981) proposed that the fault is the result of a gravitational collapse of the thickened crust, whereas McNulty and Farber (2002) suggested that the subduction of the buoyant Nazca Ridge below the Cordillera Blanca drove the footwall uplift. However, there is still no consensus on a model to explain the CBNF and the processes driving the Cordillera Blanca uplift. Margirier et al. (2015) already provided evidence for exhumation in the Cordillera Negra since 15 Ma, which is likely to be related to a regional surface uplift of the Western Andes (McLaughlin, 1924; Farrar and Noble, 1976; Myers, 1976; Wipf, 2006; Hoorn et al., 2010). The 1300 m-thick sedimentary filling of the Callejón de Huaylas suggests only low subsidence of the basin since ~5.4 Ma (Bonnot, 1984; Giovanni et al., 2010) even if the vertical displacement on the CBNF is estimated to be ~7 km (Margirier et al., 2016). In addition, our models of the landscape evolution provide new constraints on uplift rates in the Cordillera Blanca region. We suggest that the Cordillera Blanca has been uplifted in relation to the Cordillera Negra during the past 7 Ma. Observations clearly suggest that the displacement on the CBNF is mostly the result of the Cordillera Blanca uplift rather than subsidence of the hanging wall. The rock uplift evidenced in this study for the Cordillera Blanca (7–0 Ma) and proposed in the Cordillera Negra (15–0 Ma; Margirier et al., 2015) is not compatible with the collapse model proposed by Dalmayrac and Molnar (1981). Moreover, new reconstructions of the timing (15–11 Ma) and location of the initial Nazca Ridge subduction (Hampel, 2002; Rosenbaum et al., 2005; Antonijevic et al., 2015) are not compatible with the timing and location of normal faulting in the Cordillera Blanca (5.4 Ma; Bonnot, 1984; Giovanni et al., 2010). Indeed, even if the Nazca Ridge subduction initiate at 11°S, the latitude of the Cordillera Blanca between 15 and 11 Ma, at ~5 Ma, the time of initiation of normal faulting the ridge is farther south (~13°S) and at the present day the ridge is at 15°S whereas the CBNF is still active. This suggests that the Nazca Ridge did not trigger the Cordillera Blanca uplift as proposed by McNulty and Farber (2002). Our landscape evolution models do not permit to test the role of geodynamic processes such as slab flattening on the CBNF initiation and Cordillera Blanca uplift. However, the subduction geometry and change of the mechanical coupling on the subduction interface may have had an influence on the tectonic regime of the upper plate as suggested by Margirier et al. (2017) for the Cordillera Blanca region. After the initiation of normal faulting, when the Cordillera Blanca batholith started to be eroded, since ~3 Ma, the erosion of denser rocks is likely to have trigger an increase of the uplift rates along the CBNF.

6. Conclusions

Our study provides new constraints on the erosion efficiency, elastic thickness of the lithosphere, temperature gradient in the crust and uplift rates in the Andes of northern Peru. The absolute rock uplift rates obtained at the end of the models for the Cordillera Blanca (ranging from 1.5 to 2.5 mm/yr) are coherent with Quaternary slip rates documented on the CBNF (5.1 ± 0.8 mm/yr to 0.6 ± 0.2 mm/yr, Schwartz, 1988; Siame et al., 2006; Margirier et al., 2017; Gérard et al., n.d.). Our results suggest an acceleration of rock uplift in the Cordillera Blanca at 2 Ma in agreement with the increase in erosion rate evidenced by Margirier et al. (2016). We show, however, that such an increase in erosion rate may be the result of erosional unloading and isostasy rather than being related to a change in either tectonic or climatic forcing. We also show that this acceleration may have been amplified by the unroofing of a dense granitic intrusion.

Based on the present-day drainage divide location in the Cordillera Blanca and the results of our modeling, we propose that the Callejón de Huaylas was already a depression before the Cordillera Blanca batholith emplacement and that a proto Cordillera Blanca already existed at that

time.

Finally, in the light of our modeling of the landscape evolution, we show that the two models previously published for the CBNF (e.g., gravitational collapse of the thickened crust/footwall uplift due to the subduction of the Nazca Ridge; Dalmayrac and Molnar, 1981; McNulty and Farber, 2002) are inconsistent with the thermochronological data, geodynamic and geologic context. Further investigations are needed to assess if the Quaternary extensional tectonics have been triggered by flat slab subduction, which may also have triggered at the same time the uplift of the Cordillera Blanca. We suggest, however, that, in this context, the construction of high-relief topography was strongly influenced by the isostatic flexural rebound and, to some degree, by the exhumation of the dense Cordillera Blanca granite.

Supplementary data to this article can be found online at https://doi.org/10.1016/j.tecto.2018.02.009.

Acknowledgements

We thank Emily Richards for proofreading the manuscript and English improvements, Jessica Stanley and Benoît Bovy for their help with the inversions on the cluster. We acknowledge the work of the editor and of our two anonymous reviewers for their critical and helpful reviews. Last but not least, Audrey Margirier acknowledges Blockzone team for the nice boulders in Potsdam.

References

Antonijevic, S.K., Wagner, L.S., Kumar, A., Beck, S.L., Long, M.D., Zandt, G., Tavera, H., Condori, C., 2015. The role of ridges in the formation and longevity of flat slabs. Nature 524 (7564), 212–215. http://dx.doi.org/10.1038/nature14648.

Barazangi, M., Isacks, B.L., 1976. Spatial distribution of earthquakes and subduction of the Nazca plate beneath South America. Geology 4 (11), 686–692.

Beckinsale, R.D., Sanchez-Fernandez, A.W., Brook, M., Cobbing, E.J., Taylor, W.P., Moore, N.B., 1985. Rb-Sr whole rock isochron and K-Ar determination for the Coastal Batholith of Peru. In: Pitcher, W.S., Atherton, M.P., Cobbing, E.J., Beckinsale, R.D. (Eds.), Magmatism at a Plate Edge: The Peruvian Andes. Blackie Halstead press, Glasgow, pp. 177–202.

Bonnot, D., 1984. Néotectonique et tectonique active de la Cordillère Blanche et du Callejon de Huaylas (Andes nord-péruviennes), Thèse présentée pour obtenir le grade de docteur, Université de Paris-Sud, Centre d'Orsay. pp. 1–202.

Bookhagen, B., Strecker, M.R., 2008. Orographic barriers, high-resolution TRMM rainfall, and relief variations along the eastern Andes. Geophys. Res. Lett. 35 (6), L06403. http://dx.doi.org/10.1029/2007GL032011.

Braun, J., Willett, S.D., 2013. A very efficient O(n), implicit and parallel method to solve the stream power equation governing fluvial incision and landscape evolution. Geomorphology 180-181, 170–179. http://dx.doi.org/10.1016/j.geomorph.2012.10.008.

Braun, J., Van der Beek, P., Batt, G., 2006. Quantitative Thermochronology, Numerical Methods for the Interpretation of Thermochronological Data. Cambridge University Press, Cambridge, UK (258 pp).

Braun, J., Simon-Labric, T., Murray, K.E., Reiners, P.W., 2014. Topographic relief driven by variations in surface rock density. Nat. Geosci. 7, 534–540. http://dx.doi.org/10.1038/ngeo2171.

Cederbom, C.E., Sinclair, H.D., Schlunegger, F., 2004. Climate-induced rebound and exhumation of the European Alps. Geology 32 (8), 709–712. http://dx.doi.org/10.1130/G20491.1.

Cobbing, J., Pitcher, W., Baldock, J., Taylor, W., McCourt, W., Snelling, N.J., 1981. Estudio geológico de la Cordillera Occidental del norte del Perú, Instituto Geologico Minero y Metalurgico, Serie D. Estudios Especiales. 10(D). pp. 1–252.

Croissant, T., Braun, J., 2014. Constraining the stream power law: a novel approach combining a landscape evolution model and an inversion method. Earth Surf. Dyn. 2 (1), 155–166. http://dx.doi.org/10.5194/esurf-2-155-2014-supplement.

Dalmayrac, B., Molnar, P., 1981. Parallel thrust and normal faulting in peru and constraints on the state of stress. Earth Planet. Sci. Lett. 55, 473–481.

Eakin, C.M., Lithgow-Bertelloni, C., Dávila, F.M., 2014. Influence of Peruvian flat-subduction dynamics on the evolution of western Amazonia. Earth Planet. Sci. Lett. 404 (C), 250–260. http://dx.doi.org/10.1016/j.epsl.2014.07.027.

Farber, D.L., Hancock, G.S., Finkel, R.C., Rodbell, D.T., 2005. The age and extent of tropical alpine glaciation in the Cordillera Blanca, Peru. J. Quat. Sci. 20 (7–8), 759–776. http://dx.doi.org/10.1002/jqs.994.

Farrar, E., Noble, D.C., 1976. Timing of late Tertiary deformation in the Andes of Peru. Geol. Soc. Am. Bull. 87 (9), 1247–1250.

Gérard, B., L. Audin, D. Farber, S. Hall, S. Zérathe, X. Robert, A. Margirier, J. Carcaillet, S. Schwartz, Northward Increase of Quaternary Slip Rates along the Cordillera Blanca Normal Fault, Peruvian Andes, (in prep).

Giovanni, M.K., 2007. Tectonic and Thermal Evolution of the Cordillera Blanca Detachment System, Peruvian Andes: Implication for Normal Faulting in a Contractionnal Orogen, Ph.D. Thesis. University of California, Los Angeles, pp. 1–255.

Giovanni, M.K., Horton, B.K., Garzione, C.N., McNulty, B., Grove, M., 2010. Extensional basin evolution in the Cordillera Blanca, Peru: stratigraphic and isotopic records of detachment faulting and orogenic collapse in the Andean hinterland. Tectonics 29 (6), TC6007. http://dx.doi.org/10.1029/2010TC002666.

Hampel, A., 2002. The migration history of the Nazca Ridge along the Peruvian active margin: a re-evaluation. Earth Planet. Sci. Lett. 203 (2), 665–679.

Hampel, A., Hetzel, R., Densmore, A.L., 2007. Postglacial slip-rate increase on the Teton normal fault, northern Basin and Range Province, caused by melting of the Yellowstone ice cap and deglaciation of the Teton Range? Geology 35 (12), 1107–1110. http://dx.doi.org/10.1130/G24093A.1.

Henry, S.G., Pollack, H.N., 1988. Terrestrial heat flow above the Andean subduction zone in Bolivia and Peru. J. Geophys. Res. Solid Earth 93 (B12), 15153–15162.

Hetzel, R., Hampel, A., 2005. Slip rate variations on normal faults during glacial–interglacial changes in surface loads. Nature 435, 81–84.

Hodson, K.R., 2012. Morphology, Exhumation, and Holocene Erosion Rates from a Tropical Glaciated Mountain Range: The Cordillera Blanca, Peru, Department of Earth and Planetary Sciences, Unpublished Thesis. McGill University, Montreal, pp. 1–94.

Hoorn, C., et al., 2010. Amazonia through time: Andean uplift, climate change, landscape evolution, and biodiversity. Science 330 (6006), 927–931. http://dx.doi.org/10.1126/science.1194585.

Margirier, A., Robert, X., Audin, L., Gautheron, C., Bernet, M., Hall, S., Simon-Labric, T., 2015. Slab flattening, magmatism and surface uplift in the Cordillera Occidental (northern Peru). Geology 1–16. http://dx.doi.org/10.1130/G37061.1.

Margirier, A., Audin, L., Robert, X., Herman, F., Ganne, J., Schwartz, S., 2016. Time and mode of exhumation of the Cordillera Blanca batholith (Peruvian Andes). J. Geophys. Res. Solid Earth 121, 6235–6249. http://dx.doi.org/10.1002/2016JB013055.

Margirier, A., Audin, L., Robert, X., Pêcher, A., Schwartz, S., 2017. Stress field evolution above the Peruvian flat-slab (Cordillera Blanca, northern Peru). J. S. Am. Earth Sci. 77, 58–69. http://dx.doi.org/10.1016/j.jsames.2017.04.015.

McLaughlin, D.H., 1924. Geology and physiography of the Peruvian Cordillera, Departments of Junin and Lima. Bull. Geol. Soc. Am. 35, 591–632.

McNulty, B.A., Farber, D.L., 2002. Active detachment faulting above the Peruvian flat slab. Geology 30 (6), 567–570.

Montario, M.J., 2001. Exhumation of the Cordillera Blanca, Northern Peru, based on Apatite Fission Track Analysis, Department of Geology, Unpublished Thesis. Union College, Schenectady, New York, pp. 1–12.

Montgomery, D.R., 1994. Valley incision and the uplift of mountain peaks. J. Geophys. Res. Solid Earth 99 (B7), 13913–13921.

Montgomery, D.R., 2002. Valley formation by fluvial and glacial erosion. Geology 30 (11), 1047–1050.

Montgomery, D.R., Brandon, M.T., 2002. Topographic controls on erosion rates in tectonically active mountain ranges. Earth Planet. Sci. Lett. 201, 481–489.

Montgomery, D.R., Balco, G., Willett, S.D., 2001. Climate, tectonics, and the morphology of the Andes. Geology 29 (7), 579–582.

Mukasa, S.B., 1984. Comparative Pb Isotope Systematics and Zircon U-Pb Geochronology for the Coastal, San Nicolás and Cordillera Blanca Batholiths, Peru, Ph.D. Thesis. University of California, Santa Barbara, pp. 1–362.

Myers, J.S., 1976. Erosion surfaces and ignimbrite eruption, measures of Andean uplift in northern Peru. Geol. J. 11 (1), 29–44.

Perez-Gussinye, M., Swain, C.J., Kirby, J.F., Lowry, A.R., 2009. Spatial variations of the effective elastic thickness, Te, using multitaper spectral estimation and wavelet methods: examples from synthetic data and application to South America. Geochem. Geophys. Geosyst. 10 (4), 1–10. http://dx.doi.org/10.1029/2008GC002229.

Petford, N., Atherton, M.P., 1992. Granitoid emplacement and deformation along a major crustal lineament: the Cordillera Blanca, Peru. Tectonophysics 205 (1), 171–185.

Rosenbaum, G., Giles, D., Saxon, M., Betts, P.G., Weinberg, R.F., Duboz, C., 2005. Subduction of the Nazca Ridge and the Inca Plateau: insights into the formation of ore deposits in Peru. Earth Planet. Sci. Lett. 239 (1–2), 18–32. http://dx.doi.org/10.1016/j.epsl.2005.08.003.

Sambridge, M., 1999a. Geophysical inversion with a neighbourhood algorithm — I. Searching a parameter space. Geophys. J. Int. 138, 479–494.

Sambridge, M., 1999b. Geophysical inversion with a neighbourhood algorithm — II. Appraising the ensemble. Geophys. J. Int. 138, 727–746.

Schwartz, D.P., 1988. Paleoseismicity and neotectonics of the Cordillera Blanca fault zone, northern Peruvian Andes. J. Geophys. Res. Solid Earth 93 (B5), 4712–4730.

Seltzer, G.O., Rodbell, D.T., Baker, P.A., Fritz, S.C., Tapia, P.M., Rowe, H.D., Dunbar, R.B., 2002. Early warming of tropical South America at the last glacial-interglacial transition. Science 296, 1685–1686.

Sharma, P., 1997. Environmental and Engineering Geophysics. Cambridge Univ. Press, New York.

Siame, L.L., Sébrier, M., Bellier, O., Bourles, D., 2006. Can cosmic ray exposure dating reveal the normal faulting activity of the Cordillera Blanca Fault, Peru? Rev. Asoc. Geol. Argent. 61 (4), 536–544.

Small, E.E., Anderson, R.S., 1995. Geomorphically driven late Cenozoic rock uplift in the Sierra Nevada, California. Science 270, 277–278.

Smith, J.A., Finkel, R.C., Farber, D.L., Rodbell, D.T., Seltzer, G.O., 2005. Moraine preservation and boulder erosion in the tropical Andes: interpreting old surface exposure ages in glaciated valleys. J. Quat. Sci. 20 (7–8), 735–758. http://dx.doi.org/10.1002/jqs.981.

Stern, T.A., Baxter, A.K., Barrett, P.J., 2005. Isostatic rebound due to glacial erosion within the Transantarctic Mountains. Geology 33 (3), 221–224. http://dx.doi.org/10.1130/G21068.1.

Turcotte, D.L., Schubert, G., 2002. Geodynamics. Cambridge University Press (456 pp).

Whipple, K., Meade, B., 2006. Orogen response to changes in climatic and tectonic forcing. Earth Planet. Sci. Lett. 243, 218–228.

Wipf, M., 2006. Evolution of the Western Cordillera and Coastal Margin of Peru: Evidence from Low-temperature Thermochronology and Geomorphology. Department of Earth Sciences, PhD Thesis, Swiss Federal Institute of Technology Zürich, Zürich, pp. 1–163.

Wise, J.M., Noble, D.C., 2003. Geomorphic evolution of the Cordillera Blanca, Northern Peru. Boletin de la sociedad Geologica del Peru 96, 1–21.